Materials Advances

ROYAL SOCIETY OF CHEMISTRY

PAPER

View Article Online
View Journal | View Issue

Cite this: *Mater. Adv.*, 2024, 5, 1614

Chiral discrimination of L-DOPA *via* L/D-tryptophan decorated carbon quantum dots†

Aram Rezaei, *[a] Mohammed Ahmed Hamad,[b] Hadi Adibi,[c] Huajun Zheng [d] and Khdir Hamza Qadir[b]

Chiral detection plays a crucial role in drug development by ensuring the purity and efficacy of drugs. This enables researchers to accurately identify and quantify chiral molecules, thereby determining the active form of a drug and avoiding the potential side effects associated with the inactive form. Chiral carbon quantum dots (CQDs) have garnered attention in the field of biomaterials science due to their distinctive chiroptical and electronic properties, as well as their biocompatibility, ease of synthesis, excellent photostability, and convenient surface functionalization. In this study, we successfully synthesized chiral probes using a one-pot chemical synthesis process. Specifically, we synthesized chiral CQDs *via* one-step hydrothermal synthesis of L/D-tryptophan and citric acid. Comprehensive characterization techniques, including FT-IR, PL, UV-vis, XRD, circular dichroism, ^{1}H and ^{13}C NMR, FESEM, AFM, TEM, and HRTEM, were employed to characterize the chiral CQDs. Notably, to the best of our knowledge, this study represents the first instance of well-defined chiral CQDs acting as probes for the chiral detection of L-DOPA. We evaluated the PL responses of the chiral CQDs to various chiral analytes such as cysteine, tryptophan, lysine, arginine, proline, histidine, D-penicillamine, L-DOPA, and captopril. The results demonstrate a strong interaction between the chiral L/D-Trp-CQDs and L-DOPA. Interestingly, the fluorescence spectrum of the L-Trp-CQDs remained unchanged upon the addition of L-DOPA. In contrast, D-Trp-CQDs exhibited a distinct response. When L-DOPA was introduced into the D-Trp-CQD solution, a new shoulder gradually emerged at 418 nm. This indicates that the D-Trp-CQDs exhibited a linear response (R^2 = 0.99) within the concentration range of 37–4000 nM of L-DOPA. Also, the limit of quantification (LOQ) and limit of detection (LOD) were calculated to be 37 and 11.2 nM, respectively. Therefore, chiral CQDs hold significant promise for enantioselective detection in the pharmaceutical industry and in other related fields. It offers a valuable means to ensure the safety and efficacy of pharmaceutical products.

Received 25th September 2023,
Accepted 20th December 2023

DOI: 10.1039/d3ma00757j

rsc.li/materials-advances

Introduction

Parkinson's disease is a neurological disorder characterized by the progressive loss of dopaminergic neurons in the brain, which causes tremors, rigidity and the slowing of physical movement. This leads to reduced levels of dopamine, a neurotransmitter involved in the control of motor functions. Levodopa, an anti-Parkinson medication, helps to replenish dopamine levels in the brain. As Parkinson's disease progresses, the dose of levodopa needs to be adjusted.[1,2] This is because levodopa can have adverse effects if misused or incorrectly dosed. Levodopa is a chiral molecule with a carbon atom bonded to four different functional groups, resulting in two enantiomers.[3,4] The L-DOPA enantiomer is the active form responsible for the therapeutic effects, while the D-DOPA enantiomer is inactive and can even interfere with L-DOPA's action. Hence, chirality is critical in levodopa pharmacology, and the use of pure L-DOPA is essential for successful treatment. It is therefore crucial to monitor L-DOPA levels in patients and ensure the safe and effective use of the medication.[5–7] After conducting a thorough literature review, it has been found that only a few reports exist concerning the selective detection of L-DOPA. These reports encompass various methods such as colorimetric and electrochemical techniques, high-performance liquid chromatography, and spectrophotometry.[8–16] However, it

[a] *Nano Drug Delivery Research Center, Health Technology Institute, Kermanshah University of Medical Sciences, Kermanshah, Iran. E-mail: aram.rezaei@gmail.com, aram.rezaei@kums.ac.ir*
[b] *Students Research Committee, Kermanshah University of Medical Sciences, Kermanshah, Iran*
[c] *Pharmaceutical Sciences Research Center, Health Institute, Kermanshah University of Medical Sciences, Kermanshah, Iran*
[d] *Department of Applied Chemistry, Zhejiang University of Technology, Hangzhou, 310032, China*

† Electronic supplementary information (ESI) available. See DOI: https://doi.org/10.1039/d3ma00757j

is worth noting that, to the best of our knowledge, no reports have been published on the chiral detection of L-DOPA based on chiral probes. Consequently, there is a pressing need to develop straightforward sensing methods that offer high selectivity and sensitivity for the chiral detection of L-DOPA.[17]

Chiral discrimination plays a significant role in pharmacy, as it can impact the efficacy and safety of drugs. The ability of biological systems to distinguish between enantiomers of a chiral drug can lead to differences in pharmacological activity and toxicity.[18] As a result, it is essential to consider the stereochemistry of drug molecules during drug development, identify and separate enantiomers, and evaluate their pharmacological properties separately. This can help identify the optimal enantiomer or enantiomeric mixture with the desired therapeutic effects and minimal adverse effects. Chiral detection methods aim to differentiate and quantify these enantiomers. Such techniques typically utilize specialized analytical instruments like polarimeters, chiral chromatography, or spectroscopy, which can selectively interact with and analyze the distinct properties of enantiomers.[19]

Fluorescence spectroscopy has proven to be an exceptionally powerful and versatile technique for chiral detection, particularly when combined with chiral fluorescent nanomaterials. Chiral fluorescent probes are specifically designed molecules that possess inherent chirality and exhibit fluorescence properties.[20] These probes can selectively interact with chiral molecules of interest, enabling the detection and differentiation of enantiomers with high sensitivity and specificity. By incorporating chiral elements into the structure of a fluorescent probe, such as chiral centers or chiral auxiliary groups, the probe itself becomes sensitive to the chiral environment and exhibits different fluorescence responses to different enantiomers. This unique property allows the direct and efficient detection of chiral compounds, even at low concentrations.[21,22] Fluorescence spectroscopy offers high sensitivity, selectivity, and ease of use compared to other chiral detection methods. Additionally, it allows for real-time measurements, making it a valuable tool for studying drug interactions and kinetics.[23] The use of fluorescence spectroscopy for chiral detection has broad applications in pharmaceutical research and development, as it can aid in drug discovery, development, and quality control. By enabling the accurate identification and quantification of chiral compounds, chiral detection plays a vital role in drug development, environmental monitoring, and the understanding of biological processes at a molecular level.[24,25]

CQDs are nanomaterials that consist of carbon atoms arranged in a crystalline lattice structure. They are typically less than 10 nanometers in size and have unique optical and electronic properties that make them attractive for a variety of applications.[26–28] CQDs are fluorescent, meaning that they emit light when excited by a light source, and their fluorescence properties can be tuned by controlling their size, shape, and surface chemistry. They are also biocompatible, non-toxic, and have low environmental impact, making them promising candidates for biomedical and environmental applications. One potential application of CQDs is in chiral discrimination, where they can be used to distinguish between enantiomers of chiral molecules.[29,30]

Several studies have reported the use of chiral CQDs for chiral discrimination, where they have been shown to interact differently with chiral molecules, leading to differences in their fluorescence or other optical properties. For instance, in 2016, Pan and coworkers reported that (−)/(+)-sparteine endowed CQDs with chirality *via* a surface passivation method. The synthesized CQDs were demonstrated to be a chiral separation platform for the isolation of cysteine enantiomers.[31] Another group reported that L/D-cysteine-decorated CQDs *via* a one-pot hydrothermal reaction exhibited enantioselective discrimination ability to recognize an enantiomer of tartaric acid.[32] Moreover, Copur and colleagues fabricated a fluorescence probe based on L-cysteine-modified CQDs for the chiral detection of a lysine enantiomer with a LOD value of 300 nM.[33] Interestingly, the covalent attachment of bovine serum albumin on the surface of graphene quantum dots introduced a chiral electrochemical sensing platform for tryptophan isomers.[34] In 2019, Askari *et al.* demonstrated that the chiral attachment of a cysteine enantiomer on the surface of GQDs through thiol–ene click chemistry introduced a chiral probe to detect a tryptophan enantiomer.[35] Recently, a lysine enantiomer was successfully recognized based on a chiral fluorescent sensor, which was synthesized through a one-pot reaction between citric acid and L-aspartic acid.[36] Recently, Sarma and coworkers presented a simple turn-on sensor based on graphene oxide quantum dots decorated with silk-fibroin for the detection of L-DOPA in biological samples. The corresponding probe showed a linear response to L-DOPA in the range of 0–35 μM with an LOD value of 76.18 nM.[37] Therefore, understanding and addressing chiral discrimination based on CQDs is critical for the development and use of safe and effective pharmaceuticals. To the best of our knowledge, this study represents the first and only reported investigation of chiral CQDs that exhibit exceptional performance in the chiral detection of L-DOPA.[38–41] This study aimed to assess the photoluminescence (PL) responses of chiral CQDs functionalized with tryptophan isomers (L/D-Trp-CQDs) to various chiral drugs and amino acids, including cysteine, tryptophan, lysine, arginine, proline, histidine, D-penicillamine, L-DOPA, and captopril. These findings demonstrate that the chiral D-Trp-CQDs exhibited a strong interaction with L-DOPA, resulting in the emergence of a new shoulder in the range of 300 to 500 nm when excited at 220 nm. Interestingly, the fluorescence spectrum of the L-Trp-CQDs remained unaltered upon the addition of L-DOPA, whereas the D-Trp-CQDs displayed a distinctive response, leading to the appearance of a new peak in the 418 nm region within the concentration range of 37–4000 nM of L-DOPA.

Experimental section

Materials and apparatus

All chemical compounds and solvents were purchased from Sigma/Merck and they were used as received. To prepare the

samples for NMR measurements, 20 mg of L-Trp-CQDs were dissolved in D_2O. The ^1H and ^{13}C NMR spectra were obtained using a Bruker Avance DPX 300 (300 MHz) NMR spectrometer (Ettlingen, Germany). The optical and fluorescence spectra of the chiral CQDs were obtained using a PerkinElmer ls45 fluorescence spectrophotometer, and the fluorescence was recorded at room temperature. In addition, a PerkinElmer Fourier transform infrared (FT-IR) spectrometer with KBr pellets was used to record the FT-IR spectra at 400–4000 cm^{-1}. Furthermore, the TEM and HRTEM measurements were performed using a Tecnai G2 F30 instrument (Thermo Fisher Scientific). Field emission scanning electron microscopy (FESEM) was performed using a SIGMA VP 500 microscope (Zeiss). X-ray diffraction (XRD) patterns were acquired utilizing an X′PretPro diffractometer from Panalytical-Holland, employing Cu Kα radiation (λ = 1.54 A). To prepare the samples for atomic force microscopy (AFM) measurements, the corresponding product suspensions were deposited onto mica, followed by vacuum drying. The prepared samples were then examined using a scanning probe microscope (SPM) in AFM mode, specifically the DME-95-50 E model, with a Si tip featuring a tip radius of 10 nm. The examination was performed in tapping mode at a frequency of 320 kHz.

Synthesis of chiral L/D-Trp-CQDs

To produce chiral CQDs, we began by adding 1 mmol of L/D-tryptophan to 15 mL of double distilled water with stirring. The pH was increased to 9 until it was fully dissolved. Following that, 1 mmol citric acid was added and the mixture was stirred for 2 hours. The resulting clear mixture was transferred to an autoclave and heated at 180 °C for 5 hours. Subsequently, the brown mixture was centrifuged at 15 000 rpm to extract the larger particles. The CQD solution was then purified for 48 hours using a 100 Da dialysis membrane. Finally, the resulting solution was solidified through freeze drying.[42–44]

Fluorescent assay to explore the interaction between amino acids and drugs with chiral L/D-Trp-CQDs

A quartz cuvette was utilized to hold a 2 mL solution of chiral L/D-Trp-CQDs at a concentration of 200 ng mL^{-1}. A chiral analyte solution with a concentration of 300 nM was prepared in PBS (pH 7.4). Subsequently, aliquots of the analyte solution were added to the cuvette *via* pipette mixing, and incubated for 5 minutes at room temperature. The resulting fluorescence spectra were recorded between 300 and 500 nm after each addition. An excitation wavelength of 220 nm was utilized for the measurements.

Results and discussion

Synthesis and characterization of chiral L/D-Trp-CQDs

To initiate the synthesis of chiral zero-dimensional CQDs, a specific quantity of L/D-tryptophan was added to double distilled water and allowed to completely dissolve by raising the pH to 9. Subsequently, citric acid was added to the clear mixture, which was then transferred to an autoclave and heated at 180 °C for 5 hours. The resulting brown mixture was centrifuged to eliminate larger particles, and the CQDs were purified using a 100 Da dialysis membrane for 48 hours. Finally, the solution was subjected to freeze-drying to obtain the solid product. The CQDs produced utilizing L-tryptophan were identified as chiral L-Trp-CQDs, while those made with D-tryptophan were designated as D-Trp-CQDs. Fig. 1 outlines the synthesis of chiral carbon quantum dots.[26]

Fig. 2 displays the FT-IR spectrum of the chiral CQDs, revealing strong and broad O–H and N–H stretching vibrations at around 3400 cm^{-1}. The bands present in the range of 2852 to 2922 cm^{-1} are attributed to the symmetric and asymmetric stretching vibrational modes of the CH_2 and CH_3 groups, respectively. The ester and amide carbonyl stretching modes were observed at around 1590–1720 cm^{-1}, while the C=C bonds of aromatic skeletal stretching were observed at 1452 cm^{-1}. The bending bands of the alkyl groups and C=C bonds are observed around 744 cm^{-1}.[42–44] In summary, the L/D-Try-CQD spectrum demonstrates the anticipated absorption bands, indicating the successful synthesis of this material.

NMR spectroscopy is a potent method for determining the chemical structure of materials by detecting functional groups in various chemical environments. The ^1H NMR spectra (Fig. 3A) revealed peaks at 1.5–3.4 ppm, which were attributed to the aliphatic hydrogens of the alkyl groups. Additionally, the protons of the carbons attached to electron-withdrawing groups, such as N and O atoms, emerged at 3.6–4.5 ppm. Interestingly, the characteristic peaks observed at 6.8–7.8 ppm correspond to the aromatic hydrogens in the graphene sheets and aromatic rings. The ^{13}C NMR spectra of chiral L-Trp-CQDs revealed peaks at around 24.3–58.5 ppm, belonging to the methylene groups of alkyl moieties. Furthermore, the carbon atoms connected to electron-withdrawing groups display distinct signals at around 76.2 ppm. The peaks in the range of 111.0–137.1 ppm could be assigned to aromatic carbons, while the carbonyl group signals emerged at 180.3–183.1 ppm (Fig. 3B).[42–44]

TEM, which is the most sophisticated imaging technique, uncovered the graphitic nature of the carbon building blocks with high crystallinity. Additionally, the spacing of parallel crystal planes was determined to be 0.21 nm, which is in good accordance with the (002) diffraction plane of the sp^2 carbon network.[45] The diameter of L-Trp-CQDs, which was uniformly sized, was estimated to be <15 nm (Fig. 4A and B). FESEM was utilized in order to analyze the surface morphology of chiral CQDs. Based on the FESEM image depicted in Fig. 4C, it was observed that the L-Trp-CQDs had discrete, spherical particles exhibiting fine characteristics. Moreover, based on FESEM measurements, the diameter of the L-Trp-CQDs was estimated to be <10 nm (Fig. 4D). The homogeneity seen in the samples indicates that the synthesis method was optimal and that the particles were resistant to aggregation, indicating stability.[26]

AFM is a high-resolution imaging technique employed to study the nanoscale topography, thickness, degree of exfoliation, and physical properties of surfaces. Fig. 5 demonstrates that the L-Trp-CQDs exhibit remarkable uniformity in size

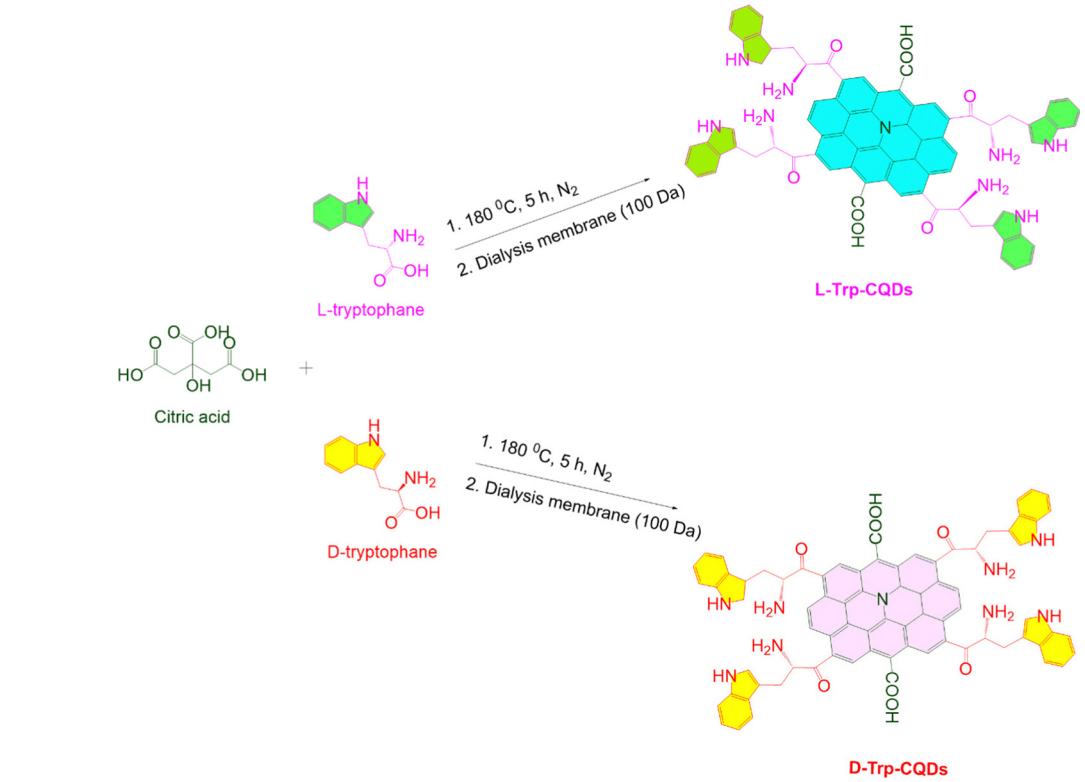

Fig. 1 Schematic diagram illustrating the synthesis of chiral carbon quantum dots from tryptophan and their subsequent purification.

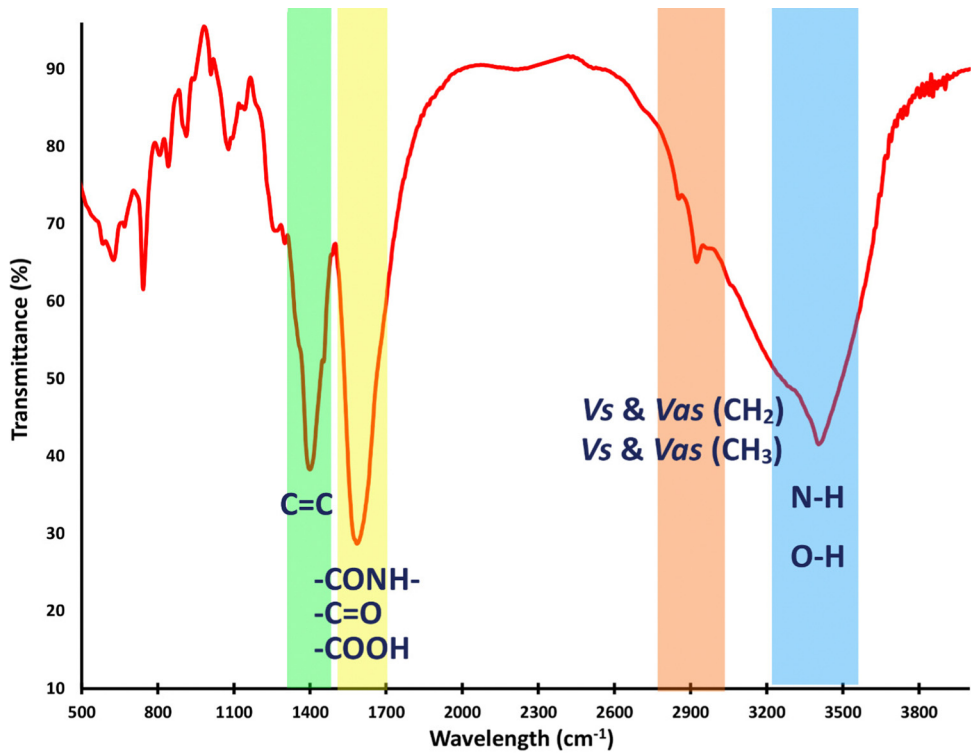

Fig. 2 FT-IR spectra of chiral L-Trp-CQDs.

and shape. The line-scanning profile further reveals a thickness of approximately 1.6 nm for the L-Trp-CQDs, which corresponds to a few layers of graphene sheets (Fig. 5A–C). Additionally, the particles exhibit a narrow size distribution, with an average

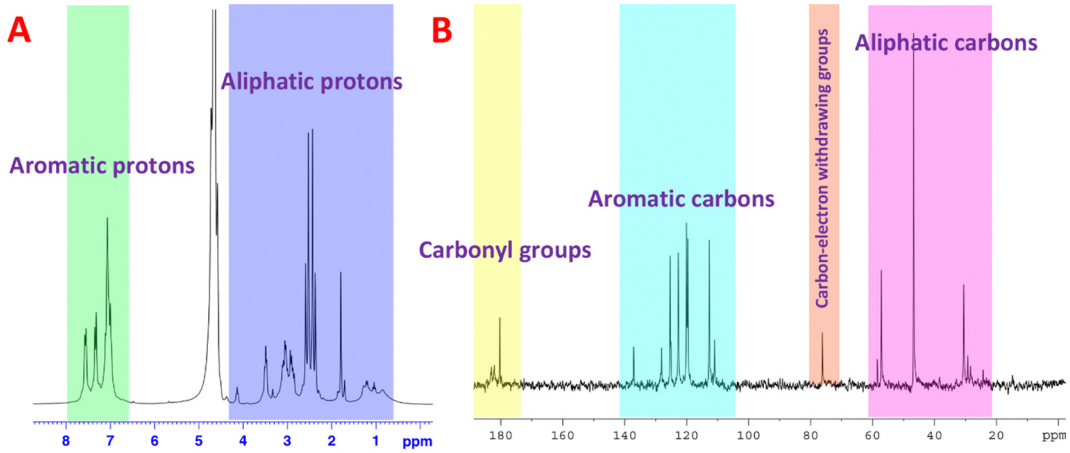

Fig. 3 Structural characterization of chiral L-Trp-CQDs by NMR spectroscopy. (A) ^{1}H NMR and (B) ^{13}C NMR spectra of CQDs in D_2O.

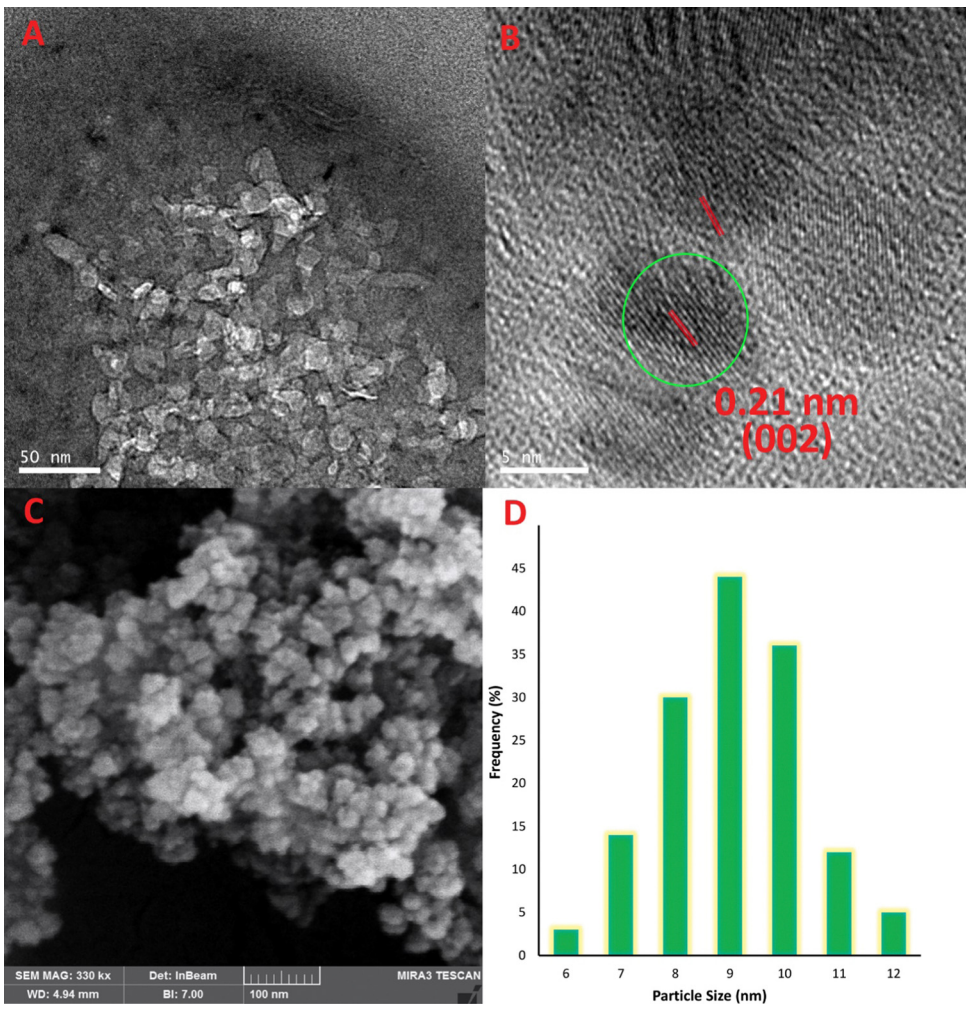

Fig. 4 (A) TEM, (B) HRTEM, and (C) FESEM images. (D) Morphological characterization of L-Trp-CQDs.

diameter of 5 nm (Fig. 5D). These findings are consistent with the TEM analysis.

Fig. 6A and B illustrate the fluorescence spectra of L-Trp-CQDs, which were excited at various wavelengths ranging from 190 to 260 nm. The PL emission of the L-Trp-CQDs was found to be the most intense at 360 nm, with an excitation wavelength of 220 nm.[26] UV-vis spectroscopy was employed to investigate the electronic structure of the L-Trp-CQDs (Fig. 6C). The aqueous

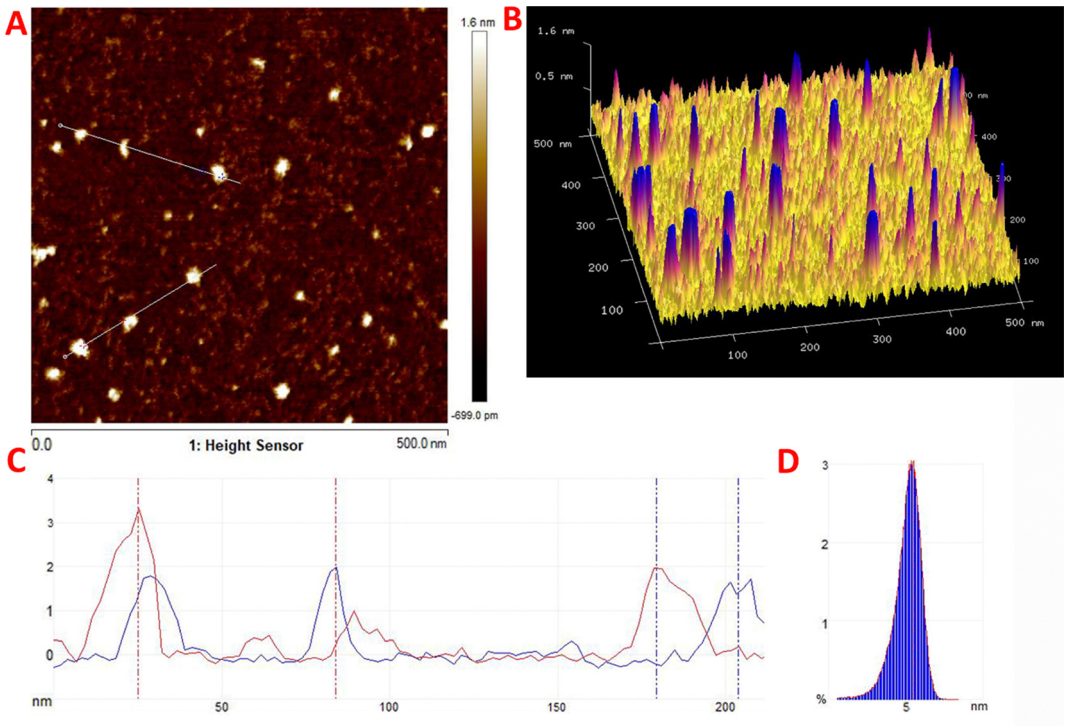

Fig. 5 (A) 2D and (B) 3D AFM plots of L-Trp-CQDs. (C) Line-scanning and (D) particle size distribution profiles of L-Trp-CQDs based on AFM.

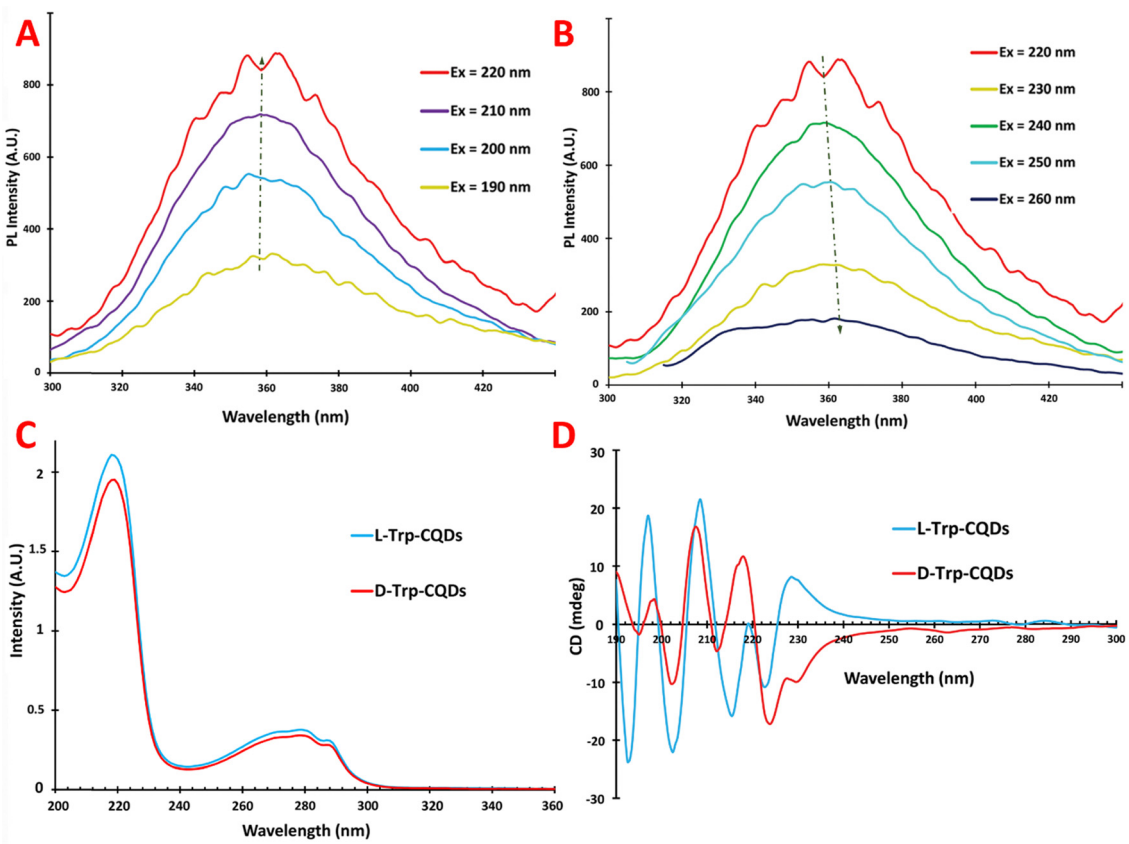

Fig. 6 Emission diagrams of L-Trp-CQDs with increasing excitation wavelengths (A) from 190 to 220 nm and (B) from 220 to 260 nm, (C) UV-vis spectrum, and (D) CD plot of L/D-Trp-CQDs.

dispersion of the sample exhibited two distinct absorption peaks: one at 218 nm and the other in the range of 245–305 nm. These absorption peaks were attributed to the $\pi \rightarrow \pi^*$ electronic transitions of the aromatic networks and $n \rightarrow \pi^*$ transitions of the heteroatom groups. Additionally, UV-vis analysis was conducted to examine the electronic structure of the counterpart enantiomer. The results revealed that the optical profile of the D-Trp-CQDs closely resembled that of L-Trp-CQDs (Fig. 6C). Additionally, to verify the generation of pseudo-enantiomeric optically active CQDs *via* the conjugation of CQDs to either L-tryptophan or D-tryptophan, circular dichroism (CD) measurements were conducted (Fig. 6D). Both L-Trp-CQDs and L-Trp-CQDs exhibited the expected pseudo-symmetry in the range of 190–300 nm. The CD spectra provided evidence of a chiral environment, indicating the presence of chirality. It can be inferred that the chirality arises from the presence of tryptophan residues on the surface of the CQDs.

Fig. S1 (ESI†) depicts the XRD patterns of the samples. Both L-Trp-CQDs and D-Trp-CQDs exhibited XRD patterns featuring a distinctive broad peak at around 22°, indicating the amorphous nature of the CQD core. The XRD profiles of the D-Trp-CQDs closely resemble those of the L-Trp-CQDs, indicating similarities in their structural characteristics. Interestingly, the XRD spectra suggest that the chirality associated with the tryptophan residue on the surface of the nanoparticles does not have a noticeable effect on the XRD pattern.

The fluorescence intensity of the CQDs in various buffers was determined by comparison with the emission intensity in double distilled water, which served as a blank (F°). The F/F° ratio was calculated to assess the effect of the buffer on the emission intensity. Different buffers were tested to evaluate their effects on the optical and emission properties of L-Trp-CQDs. The results, presented in Fig. 7A indicate that the maximal emission occurred in double distilled water, while the emission intensity decreased moderately in acetate buffer (pH 5.5). Tris–HCl buffer (pH 8.8) slightly reduced the emission intensity of the L-Trp-CQDs. However, the results indicated that PBS buffer (pH 7.4) is a suitable buffer for fluorescence spectroscopy.[13]

Chiral discrimination of L-DOPA

Investigation of the possible interaction of chiral D-Trp-CQDs with different chiral analytes

Quantum dots have been identified as useful receptors for chiral sensing applications owing to their fluorescence signaling modes. To demonstrate the performance of CQDs as photoluminescent enantioselective sensors, classical photoluminescence measurements were carried out in solution.[34,46] This method relies on changes in the photoluminescence intensity upon theaddition of the analyte, which is widely used to measure enantioselective responses. To conduct this test, a solution of 2 ml of D-Trp-CQDs at a concentration of 200 ng ml^{-1} was introduced into a quartz cuvette, and its fluorescence was measured as a blank. Different analytes were then introduced into the cuvette containing quantum dots, and their fluorescence was measured after 5 minutes of incubation. The ratio of the emission intensity of the solution to that of the blank solution was subsequently computed. Fig. 7B illustrates the PL responses of the CQDs to various analytes (F/F°), including cysteine, tryptophan, lysine, arginine, proline, histidine, D-penicillamine, L-DOPA and captopril. Notably, L-DOPA exhibited a strong interaction with D-Trp-CQDs, as evidenced by the formation of a new peak in the emission spectrum of the probe upon its introduction. These results indicate that the synthesized D-Trp-CQDs exhibit a stronger interaction with L-DOPA than with the other analytes. As a result, the enantioselective interactions of L/D-Trp-CQDs in the presence of varying concentrations of L-DOPA were subsequently examined.

Investigation of the interaction of L/D-Trp-CQDs with L-DOPA

We assessed the chiral discrimination capability of the chiral probe with respect to L-DOPA. It is worth noting that meaningful changes in the fluorescence intensity or wavelength of the probe can indicate a constructive interaction between the probe and ligand. To conduct this experiment, 2 mL of L- or D-Trp-CQDs (200 ng mL^{-1}) were introduced into the fluorescence cuvette, followed by the stepwise addition of L-DOPA and

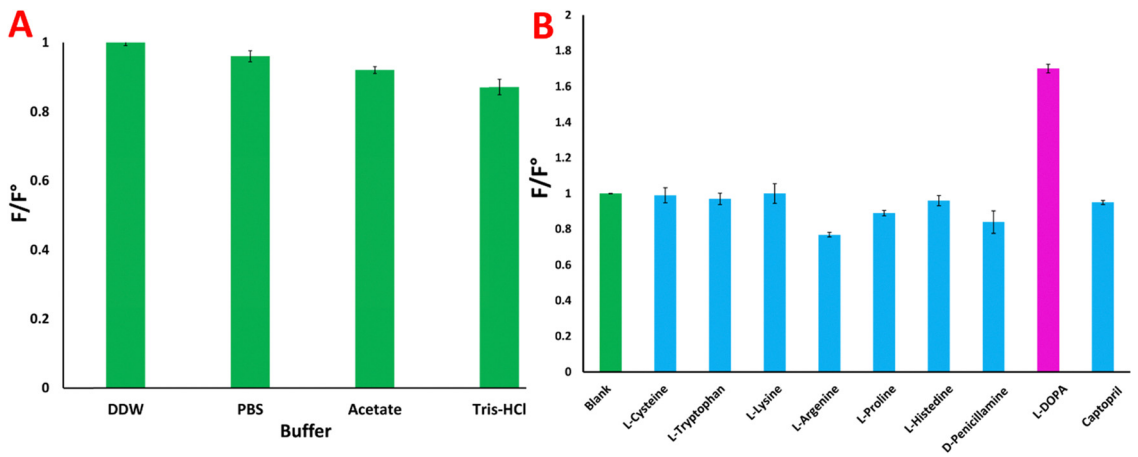

Fig. 7 (A) F/F° ratio in different buffers and (B) interaction of L-amino acids and chiral drugs with chiral D-Trp-CQDs.

incubated for 5 min. Upon gradual addition of L-DOPA to the cuvette containing L-Trp-CQDs, the fluorescence spectrum of the CQDs at 360 nm decreased slightly, but not in a linear manner, and a new peak or shoulder was not formed in the range of 300 to 500 nm. These results suggest that the interaction between the L-Trp-CQDs and L-DOPA was not stable and had no effect on the emission of the CQDs (Fig. 8A). In contrast to the L-Trp-CQDs, the D-Trp-CQDs exhibited a different response upon the introduction of L-DOPA. The results revealed that the fluorescence intensity at 360 nm did not change significantly; however, a new shoulder gradually started to appear at 418 nm as the concentration of L-DOPA increased (Fig. 8B).

To assess the analytical performance of our method, we examined the interaction behavior of D-Trp-CQDs in the presence of varying concentrations of L-DOPA. The findings revealed that as the analyte concentration increased, the emission intensity at 418 nm also increased. Eventually, when the analyte concentration reached 4000 nM, the intensity of the shoulder at 418 nm approached that of the peak at 360 nm. However, some deviations from linearity were observed at concentrations exceeding 4000 nM (Fig. S2, ESI†). Fig. 8C vividly demonstrates the competitive PL response of the L/D probes in the absence and presence of L-DOPA (4000 nM). Notably, when excited at 220 nm, the emission spectra of the L- and D-probes were almost indistinguishable (light and dark blue lines, respectively). However, upon introducing 4000 nM L-DOPA to the L-Trp-CQD probe, the emission spectrum exhibited minimal changes (orange line). In contrast, when the same amount of analyte was added to the D-Trp-CQD solution, a distinct alteration in the emission spectrum was observed, which was characterized by the emergence of a new peak at 418 nm (red line).

To establish a linear relationship between the fluorescence intensity and L-DOPA concentration, we plotted the relative PL intensities (F/F°) against the concentration of L-DOPA. The results demonstrated that D-Trp-CQDs exhibited an outstanding linear response within the concentration range of 37–4000 nM of L-DOPA, as depicted in Fig. 8D. Also, the LOQ and LOD were calculated to be 37 and 11.2 nM, respectively. The correlation coefficient (R^2) was calculated to be 0.9941.

To demonstrate the PL response to L-DOPA, L-Trp-CQD and D-Trp-CQD solutions were utilized as optical probes under UV light. The PL emission was visually observed at different concentrations of L-DOPA. Fig. 9 illustrates a significant increase in emission intensity, transitioning from light blue to dark blue,

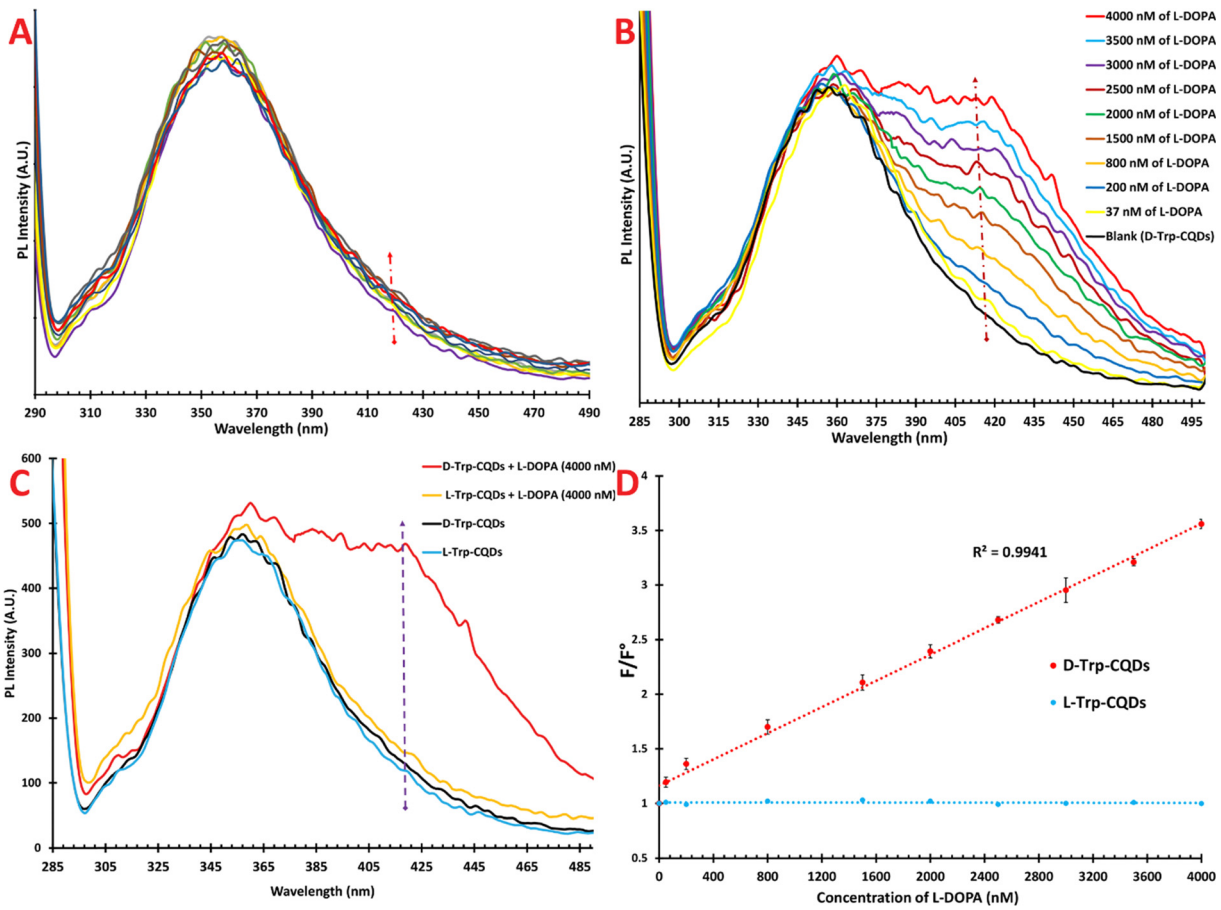

Fig. 8 PL intensities of (A) L-Trp-CQDs and (B) D-Trp-CQDs in the presence of different concentrations of L-DOPA. (C) Competitive PL response of L/D-Trp-CQDs in the absence and presence of L-DOPA (4000 nM). (D) Chiral discrimination of L-DOPA *via* L/D-Trp-CQDs.

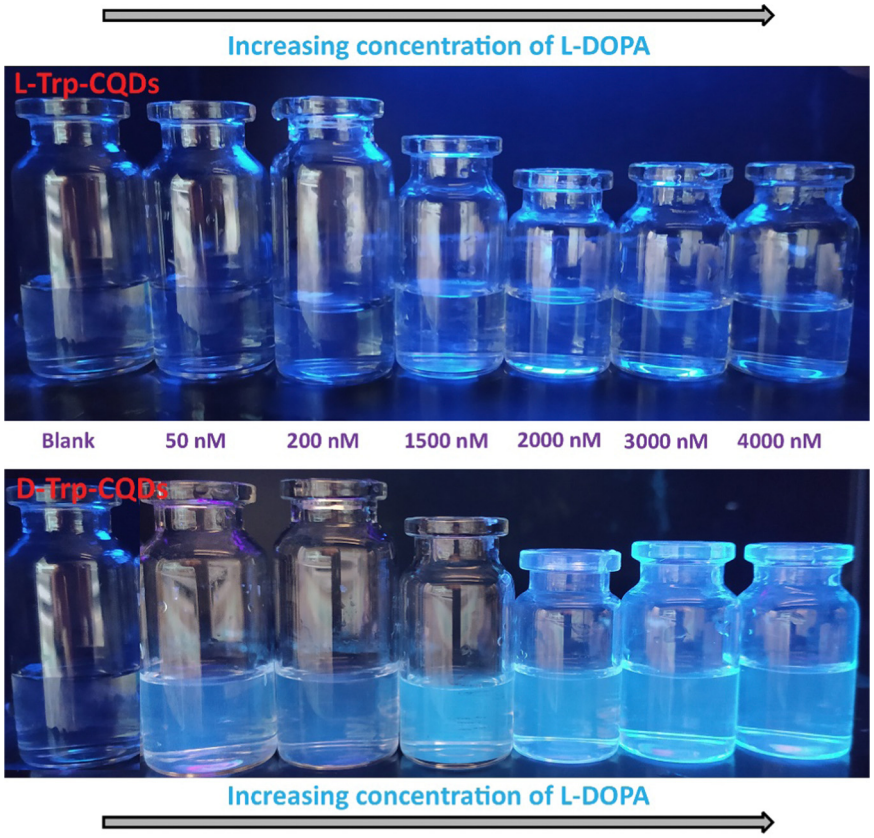

Fig. 9 PL response of L/D-Trp-CQD solutions to L-DOPA under UV light.

as the concentration of L-DOPA increased in the D-Trp-CQD solution (the so-called "turn-on" state). However, no PL change was observed in the case of the L-Trp-CQD solution, suggesting that D-Trp-CQDs enantioselectivity interacted with L-DOPA in its enantiomeric form.[33] It is evident that the enhancement in color intensity under UV light is dependent on the concentration of L-DOPA, as confirmed by the PL spectra shown in Fig. 8. The observations revealed a strong linear correlation between L-DOPA concentrations and enhancement coefficients, suggesting a logical explanation for these intriguing findings. It is plausible that the presence of hydrophilic and hydrophobic groups on the surface of chiral CQDs facilitates complex formation with L-DOPA due to their strong affinity. In terms of the mechanism underlying the turn-on states or fluorescence enhancement, upon the addition of L-DOPA within the range of 37–4000 nM, the spatial chiral complexation of L-DOPA with the surface agents of chiral CQDs is likely prioritized.[47] In the case of the D-probe, the existence of heteroatoms (*i.e.*, N and O) as chelate groups and D-tryptophan moieties on the CQD surface exhibit a strong electrostatic affinity for chiral interaction with L-DOPA. Consequently, these chiral CQDs serve as highly enantioselective and sensitive probes for the identification of L-DOPA. The enantioselective interaction between the D-Trp-CQDs and L-DOPA potentially brings two or more nanoparticles and analytes closer together, leading to the formation of dimers or increased rigidity in their structures. This rigidity in the building blocks of the chiral complex may enhance electron and charge transfer processes. As a result, the fluorescence intensity at 360 nm remains relatively unchanged, while a gradually emerging shoulder at 418 nm indicates an increase in L-DOPA concentration.[46]

Conclusion

The importance of chiral detection lies in its ability to aid in drug development and ensure the purity and efficacy of drugs. By accurately identifying and quantifying chiral molecules, researchers can determine the active form of a drug and avoid the harmful side effects associated with the inactive form. Chiral detection is therefore a critical aspect of pharmaceutical research and development, particularly for chiral drugs. Chiral CQDs have drawn attention in the field of biomaterials science because of their unique chiroptical and electronic properties, biocompatibility, ease of synthesis, excellent photostability, and facile surface functionalization. In conclusion, our study revealed that chiral probes can be synthesized effectively and affordably using a one-pot, chemical synthesis process. Specifically, chiral CQDs were synthesized *via* one-step hydrothermal synthesis of L/D-tryptophan and citric acid. We characterized the chiral CQDs using a range of comprehensive techniques, including FT-IR, PL, UV-vis, XRD, CD, ^{1}H and ^{13}C NMR, FESEM,

AFM, TEM, and HRTEM. Importantly, to the best of our knowledge, this is the first instance of well-defined chiral CQDs acting as probes for the chiral detection of L-DOPA. This study evaluated the PL responses of chiral CQDs to several chiral analytes such as cysteine, tryptophan, lysine, arginine, proline, histidine, D-penicillamine, L-DOPA, and captopril. The results showed that the chiral L/D-Trp-CQDs strongly interacted with L-DOPA. Interestingly, the fluorescence spectrum of the L-Trp-CQDs did not change upon the addition of L-DOPA. In contrast, the D-Trp-CQDs exhibited a response distinct from that of L-Trp-CQDs. Upon the introduction of L-DOPA into the D-Trp-CQD solution, a new shoulder gradually started to appear at 418 nm as the concentration of L-DOPA increased. The results indicate that D-Trp-CQDs displayed a linear response (R^2 = 0.99) in the concentration range of 37–4000 nM of L-DOPA. Therefore, the potential of chiral CQDs for enantioselective detection could have far-reaching benefits for the pharmaceutical industry and other related fields, where it is crucial to ensure the safety and efficacy of pharmaceutical products.

Author contributions

The manuscript was written through contributions of all authors. All authors have given approval to the final version of the manuscript.

Conflicts of interest

There are no conflicts to declare.

Acknowledgements

We also extend our appreciation to the Research Council of Kermanshah University of Medical Sciences for providing facilities and financial support for this work, under Grant number ''4010649''.

References

1 B. R. Bloem, M. S. Okun and C. Klein, Parkinson's disease, *Lancet*, 2021, **397**(10291), 2284–2303.
2 J. Volkmann, Deep brain stimulation for the treatment of Parkinson's disease, *J. Clin. Neurophysiol.*, 2004, **21**(1), 6–17.
3 W. Dauer and S. Przedborski, Parkinson's disease: mechanisms and models, *Neuron*, 2003, **39**(6), 889–909.
4 S. Fahn, Parkinson disease, the effect of levodopa, and the ELLDOPA trial, *Arch. Neurol.*, 1999, **56**(5), 529–535.
5 S. Fahn, The history of dopamine and levodopa in the treatment of Parkinson's disease, *Mov. Disord.*, 2008, **23**(S3), S497–S508.
6 C. W. Olanow, Y. Agid, Y. Mizuno, A. Albanese, U. Bonucelli, P. Damier, J. De Yebenes, O. Gershanik, M. Guttman and F. Grandas, Levodopa in the treatment of Parkinson's disease: current controversies, *Mov. Disord.*, 2004, **19**(9), 997–1005.
7 C. L. Tomlinson, R. Stowe, S. Patel, C. Rick, R. Gray and C. E. Clarke, Systematic review of levodopa dose equivalency reporting in Parkinson's disease, *Mov. Disord.*, 2010, **25**(15), 2649–2653.
8 I. C. César, R. M. D. Byrro, F. F. De Santana e Silva Cardoso, I. M. Mundim, L. De Souza Teixeira, S. A. Gomes, R. R. Bonfim and G. A. Pianetti, Development and validation of a high-performance liquid chromatography–electrospray ionization–MS/MS method for the simultaneous quantitation of levodopa and carbidopa in human plasma, *J. Mass Spectrom.*, 2011, **46**(9), 943–948.
9 M. Shamsipur, M. Shanehasz, K. Khajeh, N. Mollania and S. H. Kazemi, A novel quantum dot–laccase hybrid nanobiosensor for low level determination of dopamine, *Analyst*, 2012, **137**(23), 5553–5559.
10 V. Subramaniam, L. Griffith and A. J. Haes, Varying nanoparticle pseudostationary phase plug length during capillary electrophoresis, *Analyst*, 2011, **136**(17), 3469–3477.
11 K. A. Sagar and M. R. Smyth, Bioavailability studies of oral dosage forms containing levodopa and carbidopa using column-switching chromatography followed by electrochemical detection Presented at SAC 99, Dublin, Ireland, July 25–30, 1999, *Analyst*, 2000, **125**(3), 439–445.
12 J. B. Raoof, R. Ojani, M. Amiri-Aref and M. Baghayeri, Electrodeposition of quercetin at a multi-walled carbon nanotubes modified glassy carbon electrode as a novel and efficient voltammetric sensor for simultaneous determination of levodopa, uric acid and tyramine, *Sens. Actuators, B*, 2012, **166**, 508–518.
13 M. R. Hormozi-Nezhad, A. Moslehipour and A. Bigdeli, Simple and rapid detection of l-dopa based on in situ formation of polylevodopa nanoparticles, *Sens. Actuators, B*, 2017, **243**, 715–720.
14 H. Li, J. Liu, S. Guo, Y. Zhang, H. Huang, Y. Liu and Z. Kang, Carbon dots from PEG for highly sensitive detection of levodopa, *J. Mater. Chem. B*, 2015, **3**(11), 2378–2387, DOI: 10.1039/C4TB01983K.
15 D. Dăscălescu and C. Apetrei, Voltammetric Determination of Levodopa Using Mesoporous Carbon—Modified Screen-Printed Carbon Sensors, *Sensors*, 2021, **21**(18), 6301.
16 C. Chen, C. Zou, L. Li, H. Yu, J. Zhu, J. Liu and W. Huang, Blue and green emission-transformed fluorescent copolymer: Specific detection of levodopa of anti-Parkinson drug in human serum, *Talanta*, 2020, **214**, 120817, DOI: 10.1016/j.talanta.2020.120817.
17 R. D. Crapnell and C. E. Banks, Electroanalytical Overview: The Determination of Levodopa (L-DOPA), *ACS Meas. Sci. Au*, 2023, **3**(2), 84–97, DOI: 10.1021/acsmeasuresciau.2c00071.
18 P. Lazzeretti, Chiral discrimination in nuclear magnetic resonance spectroscopy, *J. Phys.: Condens. Matter*, 2017, **29**(44), 443001, DOI: 10.1088/1361-648X/aa84d5.
19 E. Mohammadi, A. Tittl, K. L. Tsakmakidis, T. Raziman and A. G. Curto, Dual nanoresonators for ultrasensitive chiral detection, *ACS Photonics*, 2021, **8**(6), 1754–1762.
20 C. M. Andersen and G. Mortensen, Fluorescence spectroscopy: A rapid tool for analyzing dairy products, *J. Agric. Food Chem.*, 2008, **56**(3), 720–729.

21 A. Belardini, E. Petronijevic, R. Ghahri, D. Rocco, F. Pandolfi, C. Sibilia and L. Mattiello, Fluorescence spectroscopy of enantiomeric amide compounds enforced by chiral light, *Appl. Sci.*, 2021, **11**(23), 11375.

22 Y. Suzuki, Y. Mizuta, A. Mikagi, T. Misawa-Suzuki, Y. Tsuchido, T. Sugaya, T. Hashimoto, K. Ema and T. Hayashita, Recognition of d-Glucose in Water with Excellent Sensitivity, Selectivity, and Chiral Selectivity Using γ-Cyclodextrin and Fluorescent Boronic Acid Inclusion Complexes Having a Pseudo-diboronic Acid Moiety, *ACS Sens.*, 2022, **8**(1), 218–227.

23 J. J. Peterson and T. D. Krauss, Fluorescence spectroscopy of single lead sulfide quantum dots, *Nano Lett.*, 2006, **6**(3), 510–514.

24 F. Zhu, J. Wang, S. Xie, Y. Zhu, L. Wang, J. Xu, S. Liao, J. Ren, Q. Liu and H. Yang, l-Pyroglutamic acid-modified CdSe/ZnS quantum dots: a new fluorescence-responsive chiral sensing platform for stereospecific molecular recognition, *Anal. Chem.*, 2020, **92**(17), 12040–12048.

25 F. Begato, R. Penasa, G. Licini and C. Zonta, Chiroptical Enhancement of Chiral Dicarboxylic Acids from Confinement in a Stereodynamic Supramolecular Cage, *ACS Sens.*, 2022, **7**(5), 1390–1394.

26 L. Hadian-Dehkordi, A. Rezaei, A. Ramazani, M. Jaymand, H. Samadian, L. Zheng, X. Deng and H. Zheng, Amphiphilic Carbon Quantum Dots as a Bridge to a Pseudohomogeneous Catalyst for Selective Oxidative Cracking of Alkenes to Aldehydes: A Nonmetallic Oxidation System, *ACS Appl. Mater. Interfaces*, 2020, **12**(28), 31360–31371, DOI: **10.1021/acsami.0c05025**.

27 M. Mohammadi, A. Khazaei, A. Rezaei, Z. Huajun and S. Xuwei, Ionic-Liquid-Modified Carbon Quantum Dots as a Support for the Immobilization of Tungstate Ions (WO42–): Heterogeneous Nanocatalysts for the Oxidation of Alcohols in Water, *ACS Sustainable Chem. Eng.*, 2019, **7**(5), 5283–5291, DOI: **10.1021/acssuschemeng.8b06279**.

28 R. Amiri, A. Rezaei, N. Fattahi, M. Pirsaheb, J. Rodríguez-Chueca and M. Moradi, Carbon quantum dots decorated Ag/CuFe2O4 for persulfate-assisted visible light photocatalytic degradation of tetracycline: A comparative study, *J. Water Process Eng.*, 2022, **47**, 102742.

29 Y. Yang, Q. Wang, G. Li, W. Guo, Z. Yang, H. Liu and X. Deng, Cysteine-Derived Chiral Carbon Quantum Dots: A Fibrinolytic Activity Regulator for Plasmin to Target the Human Islet Amyloid Polypeptide for Type 2 Diabetes Mellitus, *ACS Appl. Mater. Interfaces*, 2023, **15**(2), 2617–2629.

30 X. Li and X. Zhu, Preparation of Chiral Carbon Quantum Dots and its Application, *J. Fluoresc.*, 2023, 1–13.

31 G. Vulugundam, S. K. Misra, F. Ostadhossein, A. S. Schwartz-Duval, E. A. Daza and D. Pan, (−)/(+)-Sparteine induced chirally-active carbon nanoparticles for enantioselective separation of racemic mixtures, *Chem. Commun.*, 2016, **52**(47), 7513–7516, DOI: **10.1039/C6CC02525K**.

32 Y. Zhang, L. Hu, Y. Sun, C. Zhu, R. Li, N. Liu, H. Huang, Y. Liu, C. Huang and Z. Kang, One-step synthesis of chiral carbon quantum dots and their enantioselective recognition, *RSC Adv.*, 2016, **6**(65), 59956–59960, DOI: **10.1039/C6RA12420H**.

33 F. Copur, N. Bekar, E. Zor, S. Alpaydin and H. Bingol, Nanopaper-based photoluminescent enantioselective sensing of L-Lysine by L-Cysteine modified carbon quantum dots, *Sens. Actuators, B*, 2019, **279**, 305–312, DOI: **10.1016/j.snb.2018.10.026**.

34 Q. Ye, L. Guo, D. Wu, B. Yang, Y. Tao, L. Deng and Y. Kong, Covalent functionalization of bovine serum albumin with graphene quantum dots for stereospecific molecular recognition, *Anal. Chem.*, 2019, **91**(18), 11864–11871.

35 F. Askari, A. Rahdar and J. F. Trant, l-tryptophan adsorption differentially changes the optical behaviour of pseudo-enantiomeric cysteine-functionalized quantum dots: Towards chiral fluorescent biosensors, *Sens. Bio-Sens. Res.*, 2019, **22**, 100251, DOI: **10.1016/j.sbsr.2018.100251**.

36 P. Gao, Z. Xie and M. Zheng, Chiral carbon dots-based nanosensors for Sn(II) detection and lysine enantiomers recognition, *Sens. Actuators, B*, 2020, **319**, 128265, DOI: **10.1016/j.snb.2020.128265**.

37 K. J. Goswami, A. Boruah and N. Sen Sarma, Smart-Phone-Assisted Optical Biosensors Based on Silk-Fibroin-Decorated Reduced Graphene Oxide Quantum Dots for Fluorescent Turn-On Recognition of l-Dopa, *ACS Appl. Nano Mater.*, 2023, **6**(12), 10191–10201.

38 J. Niu, L. Rao, P. Liu, W. Zhang, W. Zhang, Y. Zuo, K. Chai, S. Chen, J. Xu and X. Duan, Chiral recognition of dihydroxyphenylalanine enantiomers with (R)/(S)-2-Phenylpropionic acid grafted PProDOT electrochemical sensors, *Synth. Met.*, 2018, **246**, 282–288, DOI: **10.1016/j.synthmet.2018.11.008**.

39 Z. Dai, J. Guo, C. Zhao, Z. Gao and Y.-Y. Song, Fabrication of Homochiral Metal–Organic Frameworks in TiO2 Nanochannels for In Situ Identification of 3,4-Dihydroxyphenylalanine Enantiomers, *Anal. Chem.*, 2021, **93**(33), 11515–11524, DOI: **10.1021/acs.analchem.1c01903**.

40 H. Sun; D. F. Hu; L. Q. Dong; X. F. Zhu; Y. S. Zhang; H. K. Xing and X. M. Duan, *Poly(3,4-Ethylenedioxythiophene) Derivatives with Electrochemical Chiral Sensor for 3,4-Dihydroxyphenylalanine Discrimination*, *Proceedings of the 2015 International Conference on Materials Chemistry and Environmental Protection (meep-15)*, 2016/03, 2016, Atlantis Press, pp 29–32, DOI: **10.2991/meep-15.2016.8**.

41 L. Zhang, C. Xu, G. Song and B. Li, Self-assembly of l-cysteine–gold nanoparticles as chiral probes for visual recognition of 3,4-dihydroxyphenylalanine enantiomers, *RSC Adv.*, 2015, **5**(34), 27003–27008, DOI: **10.1039/C5RA01271F**.

42 A. Rezaei, Y. Mohammadi, A. Ramazani and H. Zheng, Ultrasound-assisted pseudohomogeneous tungstate catalyst for selective oxidation of alcohols to aldehydes, *Sci. Rep.*, 2022, **12**(1), 3367.

43 A. Rezaei, L. Hadian-Dehkordi, H. Samadian, M. Jaymand, H. Targhan, A. Ramazani, H. Adibi, X. Deng, L. Zheng and H. Zheng, Pseudohomogeneous metallic catalyst based on tungstate-decorated amphiphilic carbon quantum dots for selective oxidative scission of alkenes to aldehyde, *Sci. Rep.*, 2021, **11**(1), 4411, DOI: **10.1038/s41598-021-83863-0**.

44 A. Rezaei and E. Hashemi, A pseudohomogeneous nanocarrier based on carbon quantum dots decorated with arginine as an efficient gene delivery vehicle, *Sci. Rep.*, 2021, **11**(1), 13790, DOI: **10.1038/s41598-021-93153-4**.

45 J.-K. Lee, J.-G. Kim, K. P. S. S. Hembram, Y.-I. Kim, B.-K. Min, Y. Park, J.-K. Lee, D. J. Moon, W. Lee, S.-G. Lee and P. John, The Nature of Metastable AA′ Graphite: Low Dimensional Nano- and Single-Crystalline Forms, *Sci. Rep.*, 2016, **6**(1), 39624, DOI: **10.1038/srep39624**.

46 X. Zeng, L. Zhang, J. Yang, Y. Guo, Y. Huang, H. Yuan and Y. Xie, A novel carbon dots derived from reduced l-glutathione as fluorescent probe for the detection of the l-/d-arginine, *New J. Chem.*, 2017, **41**(24), 15216–15228, DOI: **10.1039/C7NJ03320F**.

47 S. Jagadeeswari, M. Asha Jhonsi, A. Kathiravan and R. Renganathan, Photoinduced interaction between MPA capped CdTe QDs and certain anthraquinone dyes, *J. Lumin.*, 2011, **131**(4), 597–602, DOI: **10.1016/j.jlumin.2010.10.037**.